

## Accepted Manuscript

Identification of 5-Benzylidene-2-phenylthiazolones as Potent PRMT5 Inhibitors by Virtual Screening, Structural Optimization and Biological Evaluations

Kongkai Zhu, Hongrui Tao, Jia-Li Song, Lu Jin, Yuanyuan Zhang, Jingqiu Liu, Zhifeng Chen, Cheng-Shi Jiang, Cheng Luo, Hua Zhang

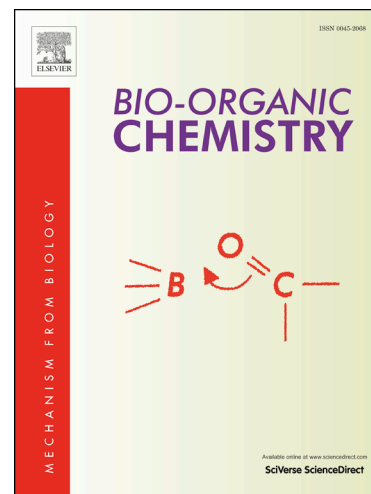
PII: S0045-2068(18)30654-0  
DOI: <https://doi.org/10.1016/j.bioorg.2018.08.021>  
Reference: YBIOO 2478

To appear in: *Bioorganic Chemistry*

Received Date: 2 July 2018  
Revised Date: 13 August 2018  
Accepted Date: 14 August 2018

Please cite this article as: K. Zhu, H. Tao, J-L. Song, L. Jin, Y. Zhang, J. Liu, Z. Chen, C-S. Jiang, C. Luo, H. Zhang, Identification of 5-Benzylidene-2-phenylthiazolones as Potent PRMT5 Inhibitors by Virtual Screening, Structural Optimization and Biological Evaluations, *Bioorganic Chemistry* (2018), doi: <https://doi.org/10.1016/j.bioorg.2018.08.021>

This is a PDF file of an unedited manuscript that has been accepted for publication. As a service to our customers we are providing this early version of the manuscript. The manuscript will undergo copyediting, typesetting, and review of the resulting proof before it is published in its final form. Please note that during the production process errors may be discovered which could affect the content, and all legal disclaimers that apply to the journal pertain.



# Identification of 5-Benzylidene-2-phenylthiazolones as Potent PRMT5 Inhibitors by Virtual Screening, Structural Optimization and Biological Evaluations

Kongkai Zhu<sup>§,†</sup>, Hongrui Tao<sup>§,†,‡</sup>, Jia-Li Song<sup>§,‡</sup>, Lu Jin<sup>#</sup>, Yuanyuan Zhang<sup>†</sup>, Jingqiu Liu<sup>†</sup>, Zhifeng Chen<sup>†</sup>, Cheng-Shi Jiang<sup>§,\*</sup>, Cheng Luo<sup>†,\*</sup> and Hua Zhang<sup>§,\*</sup>

*§School of Biological Science and Technology, University of Jinan, Jinan 250022, P.R. China;*

*#Institute of Pharmacology of Natural Products & Clinical Pharmacology, Ulm University, Germany;*

*†Drug Discovery and Design Center, State Key Laboratory of Drug Research, Shanghai Institute of Materia Medica, Chinese Academy of Sciences, Shanghai 201203, P.R. China*

\*Correspondence: Cheng-Shi Jiang, E-mail: jiangchengshi-20@163.com; Cheng Luo, E-mail: cluo@simm.ac.cn; Hua Zhang, E-mail: bio\_zhangh@ujn.edu.cn

<sup>†</sup>These authors contributed equally.

## Abstract

Protein arginine methyltransferase 5 (PRMT5) is an epigenetics related enzyme that has been validated as an important therapeutic target for glioblastoma and mantle cell lymphoma. In the present study, 11 novel PRMT5 inhibitors with 5-benzylidene-2-phenylthiazolone scaffold were identified by molecular docking-based virtual screening and structural optimization. Their IC<sub>50</sub> values against PRMT5 at enzymatic level were ranging from 0.77 to 23  $\mu$ M. As expected, the top two active hits (**5** and **19**) showed potent anti-proliferative activity against MV4-11 cells with EC<sub>50</sub> values lower than 10  $\mu$ M and reduced the cellular symmetric arginine dimethylation levels of SmD3 protein. Besides, **5** and **19** demonstrated the mechanism of cell killing in cell cycle arrest and apoptotic effect. The probable binding modes of the two compounds were explored and further verified by molecular dynamics simulation. The structure-activity relationship (SAR) of this class of structures was also discussed and further demonstrated by molecular docking simulation.

Keywords: PRMT5 inhibitor; arginine methylation; virtual screening; molecular docking, molecular dynamics simulation

## Introduction

Protein arginine methyltransferase 5 (PRMT5) belongs to an important family of enzymes that mediate gene transcription and cellular signaling by catalyzing the methylation of arginine residues of their substrates.<sup>1</sup> Using S-adenosyl-L-methionine (SAM) as the methyl donor, PRMT5 catalyzes the symmetric dimethylation of its histone and non-histone substrates assisted by its partner WD repeat protein MEP50 (methylosome protein 50, also known as Wdr77).<sup>2</sup> PRMT5 can silence the transcription of regulatory genes by methylating the H3 residue Arg8 (H3R8me2S) and H4 residue Arg3 (H4R3me2S) of histones.<sup>3,4</sup> Recently, studies have indicated that PRMT5 is a promising anticancer target for many human malignancies.<sup>5-8</sup> For example, upregulation of PRMT5 was observed in mantle cell lymphoma (MCL) patient samples, and knockdown of PRMT5 elicited potent antiproliferative effects in

MCL cell lines.<sup>4,9-11</sup> In addition, genetic attenuation of PRMT5 resulted in cell-cycle arrest, apoptosis, and loss of cell migratory activity of glioblastoma cells.<sup>7</sup> In lung cancer cells, PRMT5 was reported to promote cell proliferation by regulating multiple signaling pathways.<sup>6</sup> As a consequence, lots of efforts have been made to develop modulators of PRMT5. Encouragingly, one PRMT5 inhibitor **GSK-3326595** (Fig. 1) has been put into phase I clinical trial to study the dose escalation in subjects with solid tumors (glioblastoma, triple negative breast cancer and metastatic transitional cell carcinoma of the bladder) and non-Hodgkin's lymphoma. However, limited numbers of PRMT5 inhibitors with only five different scaffolds (Fig. 1) have been discovered so far. Considering the relatively poor druggability and lack of selectivity of the reported PRMT5 inhibitors, there is an urgent need to discover more novel PRMT5 inhibitors.

As shown in the crystal structure of human PRMT5 (Fig. S1), there are two binding sites (SAM and substrate binding sites) that can be used for the discovery of new inhibitors. Therefore, two strategies can be applied to perform structure-based virtual screening; one is targeting SAM binding site and the other is targeting substrate binding site. Accordingly, the previously reported PRMT5 inhibitors can be divided into two types. For example, **DC\_Y134**<sup>12</sup> and the pan-methyltransferase inhibitor sinefungin<sup>13</sup> (Fig. 1) belong to the SAM binding site group, while **GSK-3326595**, **EPZ015666**<sup>5</sup> and **DC-C01**<sup>14</sup> (Fig. 1) pertain to the substrate binding site class. Although it is difficult to identify potent inhibitors that could compete with SAM, many attempts have been made to identify inhibitors that could bind to SAM binding site, and two scaffolds (**17**<sup>15</sup> and **P5i-6**<sup>16</sup>) of non-SAM analogues have been reported up to now.

In the present work, a novel small-molecule PRMT5 inhibitor (**P16**) with 5-benzylidene-2-phenylthiazolone scaffold was initially identified by molecular docking-based virtual screening and showed an IC<sub>50</sub> value of 13.9  $\mu$ M in the bioassay. Further substructure search in SPECS database and structural optimization from **P16**

returned 44 extra analogues, ten of which displayed promising PRMT5 inhibitory activity with  $IC_{50}$  values ranging from 0.77 to 23  $\mu$ M. The structure-activity relationship (SAR) of these structures was elucidated. Besides, the probable binding modes of the top two active compounds **5** and **19** were explored by molecular docking and molecular dynamics simulations. Moreover, **5** and **19** also exhibited significant anti-proliferative activity against MV4-11 leukemia cells and altered the endogenous arginine methylation level of SmD3, a protein that could be used to track the cell biochemical activity of PRMT5.<sup>17-19</sup> The scaffold discovered in this work can be further optimized and used as a chemical probe to investigate the functions of PRMT5.

## Results and discussion

### Molecular docking-based virtual screening leading to the discovery of the hit compound P16.

Currently, ten X-ray crystal structures of human PRMT5 are available in RCSB protein data bank (PDB) with codes 4X60,<sup>5</sup> 4X61,<sup>5</sup> 4X63,<sup>5</sup> 4GQB,<sup>13</sup> 5C9Z, 5EMJ,<sup>20</sup> 5EMK,<sup>20</sup> 5EML,<sup>20</sup> 5EMM,<sup>20</sup> and 5FA5,<sup>21</sup> which enables the feasibility of molecular docking-based virtual screening. In order to build an optimum structural model to perform molecular docking, these crystal structures were carefully analyzed and a model containing PRMT5:MEP50, SAM and H4 peptide was finally constructed. Briefly, the crystal structure with PDB code 5EML comprising the cofactor SAM was chosen as template to build the PRMT5:MEP50 and SAM fragments, while 4GQB which was the only one containing a H4 peptide in substrate binding site was chosen as the template to construct the H4 peptide part. In the constructed structure model, the coordinates of PRMT5:MEP50 and SAM were originated from 5EML while the H4 peptide was originated from 4GQB. Docking SAM to its binding site could well reproduce the binding mode resolved by the crystal structure, which supported the reliability of the current virtual screening method. In addition, a small library containing 20 small-molecule PRMT5 inhibitors (analogues of **17** and **P5i-6**,  $IC_{50}$  < 10  $\mu$ M) and 780 decoys were manually prepared to test the enrichment capability of

the docking method. All the 20 active compounds were found in top 10% range ranked by XP Gscore when screening this library, which further validated the reliability and effectiveness of the method.

SPECS database (<http://www.specs.net>) containing 212,255 compounds were screened *in silico* to obtain candidates that showed potent binding affinity with PRMT5, and the top 1000 compounds ranked by XP Gscore were retained for visual inspection to retrieve compounds possessing well chemical fitness with SAM binding site and diverse chemical scaffolds. After filtration by “Lipinski’s Rule of Five” and clustering with “Clustering Molecules” protocol by Pipeline Pilot 7.5, 40 molecules were selected and purchased for subsequent biological evaluation at enzymatic level (Fig. 2A, the virtual screening workflow). Among them, one hit compound (**P16**) displayed the best inhibitory activity (Table S1) when tested by the Alpha LISA method<sup>15</sup> with an IC<sub>50</sub> value of 13.9 μM (Fig. 2B).

### Hit optimization returned the submicromolar active lead compound 5

Similarity-based analogue search and synthetic structural optimization were carried out to improve the potency of the hit compound **P16**. Substructure search method was used to do similarity-based analogue search and retrieved 19 analogues in SPECS database. Meanwhile, structural optimization afforded 25 additional analogues. The latter 25 compounds were smoothly synthesized by one-pot reaction according to a previously reported protocol<sup>22</sup> using the reagents including 4-methylbenzonitrile, 2-mercaptoacetic acid and substituted benzaldehydes in hand. The synthetic route was outlined in Scheme 1. The double bond configuration of the synthesized compounds was assigned to be *Z* based NMR and HPLC analyses and similar structural analogues were also reported with *Z* geometry in the literature.<sup>22</sup>



**Scheme 1.** Synthesis of thiazolone-based **P16** analogues. Reagents and conditions:

Et<sub>3</sub>N, MeOH or EtOH, reflux, 12 h.

The total of 44 compounds was then tested *in vitro* for their inhibitory activities against PRMT5. The inhibition rates at 50 μM were first obtained and the IC<sub>50</sub> values of those with >40% inhibition rate were further determined (Table 1). Alpha LISA assay identified ten active compounds with IC<sub>50</sub> values ranging from 0.77 to 23 μM. The structure-activity relationship (SAR) of this series of compounds was discussed below.

Clearly, compounds showing inhibition rate above 40% at 50 μM were found to have at least one hydroxyl group on the benzene ring (R<sup>2</sup>), and those without the hydroxyl substituent were inactive. This obviously indicated that the presence of hydroxyl group as hydrogen bond donor or acceptor played a key role in their activity, which was lately validated by the predicted binding mode from molecular docking. In addition, comparison of activities between the compounds with R<sup>1</sup> as methyl and as H suggested that the presence of methyl (R<sup>1</sup>) was not necessary. For example, each pair of active compounds **14/41**, **22/44** and **42/P16** showed similar activity toward PRMT5. In most cases, the alkylation of hydroxyl(s) at *meta*- and/or *ortho*-position of benzene ring reduced the activity, which was reflected by the inhibition rates of compounds **3-18**. It was worth noting that the introduction of a halogen element (*e.g.*, Cl or Br) in **14**, **16**, **20** and **41** increased their PRMT5 inhibitory activity compared with **6**, suggesting that the halogen atom was also vital to the activity in the condition of the presence of hydroxyl group(s). Meanwhile, substitution of Cl and Br seemed to have a similar effect on the compounds' activity (**16** vs **20**).

Next, the IC<sub>50</sub> values of compounds **5**, **14-16**, **19**, **20**, **22**, **41**, **42**, and **44** for PRMT5 inhibition were tested. Most of the compounds showed the same level activity to **P16** with IC<sub>50</sub> values ranging from 11.0 to 23.0 μM. Among them, two analogues **5** and **19** displayed significantly improved activity with IC<sub>50</sub> values of 0.77 and 6.60 μM, respectively (Fig. 3A).

**Compound 5 showed selective inhibitory activity against PRMT5.**

The most active **5** was chosen for further test on its inhibition against the other key homological member of PRMT5, PRMT1. As shown in Fig. S2, the assay results ( $IC_{50} = 10.0 \mu\text{M}$ ) revealed that **5** was displayed moderate selectivity (13-fold) against PRMT5.

**Predicted binding modes with PRMT5 of the top two active compounds**

Compounds **5** and **19** showed the best inhibitory activity against PRMT5 among all tested analogues, and their binding modes with PRMT5 were thus analyzed. As shown in Fig. 3B–3C, the two compounds showed similar binding modes with quite consistent space orientations. Hydrophobic, hydrogen bond, cation- $\pi$ , and  $\pi$ - $\pi$  interactions were observed and contributed to the binding affinity by further analysis (Fig. 4). Both compounds **5** and **19** were located in the hydrophobic pocket which is composed of residues Y324, L319, P314, L315, L436, M420 and A366 (Fig. 4). In particular, the methylbenzene ring established cation- $\pi$  interaction with the side chain of K393. Not surprisingly, all hydroxyl groups in the two compounds formed hydrogen bonds with residues G365 of PRMT5, indicative of their important contribution to the activity. By comparing the binding modes of the two compounds with that of SAM (Fig. S3), we concluded that this series of compounds could efficiently occupy the SAM binding pocket of PRMT5.

In order to further validate their binding modes, 100 ns molecular dynamics simulations were conducted on the two binding poses. The interactions between each compound and PRMT5 were found to be stable during the MD simulation process by analyzing the root mean square deviation (RMSD) values of each MD trajectory (Fig. S4 and S5). As the two compounds showed equivalent XP Gscore, the binding free energies of **5** and **19** with PRMT5 were calculated by MM/PBSA method with values of  $-31.85 \text{ kcal/mol}$  and  $-27.34 \text{ kcal/mol}$ , respectively. The results were in well accordance with their experimental activity data.



### **Anti-proliferative and cellular symmetric dimethylation effects of **5** and **19** on leukemia cell line MV4-11**

Leukemia cell line MV4-11 was used to measure the anti-proliferative effects of **5** and **19**, and the results were summarized in Fig. 5A. The two compounds showed a dose- and time-dependent manner in inhibiting MV4-11 cell proliferation with 12-day EC<sub>50</sub> values of 7.93  $\mu$ M and 3.30  $\mu$ M, respectively. It was interesting to note that **5** displayed more potent inhibitory activity than **19** at enzymatic level but was less active at cell level. This observation could result from the higher cell membrane permeability of **19** as indicated by its better *ClogP* parameter (2.50) than that (4.03) of **5**.

The effects of **5**, **19** and **EPZ015666** (positive control) on cellular symmetric arginine dimethylation in MV4-11 cells (Fig. 5B and Fig. S6) were tested by immunoblot using symmetric dimethyl arginine (SDMA) antibody. Similarly to **EPZ015666**, treatment of **5** and **19** led to a concentration dependent decrease in the intensity of multiple bands, including PRMT5 substrate SmD3 protein. Concentration-dependent decreases in SmD3me<sub>2</sub>s were observed, which demonstrated the PRMT5 engagement effects of the compounds in a cellular context.

### **Inducement of cell cycle arrest and cell apoptosis of **5** and **19****

The effects of **5** and **19** on cell cycle and cell apoptosis were examined to illustrate their anti-proliferation mechanism through flow cytometric analysis. The results showed a concentration-dependent cell cycle arrest at G1 phase (Fig. 6 and Fig. S7) and increased apoptosis (Fig. 7 and Fig. S8) upon treatment with the two compounds for 24 and 48 hours, respectively. These results were in agreement with the critical role of PRMT5 in glioblastoma differentiated cells (GBMDC) and glioblastoma neurospheres (GBMNS), which uncovered that PRMT5 knockdown in GBMDC led to cell apoptosis and knockdown in GBMNS led to G1 cell cycle arrest.<sup>23</sup> These findings indicated that this series of compounds were both cell-cycle arrestors and

apoptosis inducers.

## Experimental methods

### Molecular docking-based virtual screening

Among the ten determined X-ray crystal structures of human PRMT5, 5EML and 4X61 are the two structures containing the cofactor SAM, while 4GQB is the only one that comprises a histone H4 peptide in substrate binding site with a PRMT5 inhibitor occupying SAM binding site. Therefore, 4GQB and 5EML with higher resolution (2.39 Å) than 4X61 (2.85 Å) were chosen to construct the structure model for virtual screening targeting SAM binding site. By superposing 5EML with 4GQB and replacing the coordinates of the substrate binding site inhibitor **5QK** in 5EML with H4 peptide in 4GQB, a new complex model containing PRMT5:MEP50, SAM and H4 peptide was finally obtained and used for further study. In this constructed complex model, all the coordinates were derived from 5EML except for the H4 peptide. The docking simulation was performed using Schrödinger software running under Maestro version 7.5. Glide program<sup>24, 25</sup> embedded in Maestro 7.5 was used to carry out molecular docking. During the docking process, the coordinates of the protein (PRMT5:MEP50 and H4 peptide) were first minimized using the Protein Preparation Wizard Workflow with default settings, and docking grids were then created by defining residues within 15 Å around SAM. Finally, compounds of SPECS database prepared by the LigPrep panel (version 2.3, Schrödinger, LLC, New York, NY) were docked into the well-defined docking grids with the extra precision (XP) mode.

### Chemistry

All purchased compounds were from commercial supplier (SPECS database) and used without further purification. Purity of these compounds was  $\geq 95\%$  as declared by the chemical vendor (Table S1–S2).

**General methods.** Melting points were measured on a RY-1 melting point apparatus

(Tianjin Analysis Instrument Factory, Tianjin, China). Commercially available reagents were used without further purification. Organic solvents were evaporated under reduced pressure using a Büchi R-100 evaporator. Reactions were monitored by TLC using GF<sub>254</sub> pre-coated silica gel plates (Yantai JiangYou Silica Gel Inc., Yantai, China). Column chromatography was performed on 200–300 mesh silica gel (Qingdao Marine Chemical Inc., Qingdao, China). NMR spectra were acquired on a Bruker AVANCE DRX600 spectrometer. Chemical shifts were expressed in  $\delta$  (ppm) and coupling constants ( $J$ ) in Hz using solvent signals as references (CDCl<sub>3</sub>,  $\delta_{\text{H}}$  7.26 ppm and  $\delta_{\text{C}}$  77.23 ppm; CD<sub>3</sub>OD,  $\delta_{\text{H}}$  3.31 ppm and  $\delta_{\text{C}}$  49.00 ppm; DMSO-*d*<sub>6</sub>,  $\delta_{\text{H}}$  2.50 ppm and  $\delta_{\text{C}}$  39.50 ppm). The purity of the samples was determined by analytical HPLC using an Agilent 1260 system with ZDRBAX SB-C18 column (4.6 mm  $\times$  150 mm). HPLC data were recorded using parameters as follows: H<sub>2</sub>O/MeOH, 60/40 to 0/100 in 30 min, +30 min isocratic, flow rate of 1.0 mL/min,  $\lambda$  = 280 and 320 nm. High-resolution mass spectra (HRMS) were recorded on an Agilent Q-TOF 6520 MS spectrometer.

*General procedure for synthesis of 5-benzylidene-2-phenylthiazolones 1-8, 10, 11, and 23-37.* A solution of *p*-methylbenzonnitrile (117 mg, 1 mmol), thioglycolic acid (101 mg, 1.1 mmol), corresponding benzaldehyde (1 mmol) and 0.5 mL triethylamine in 5 mL methanol or ethanol was refluxed for at least 12 h. The reaction mixture was evaporated under reduced pressure, and the residue was purified by silica gel column chromatography to afford the desired product.

*(Z)*-5-Benzylidene-2-(*p*-tolyl)thiazol-4(5*H*)-one (**1**)

A yellow solid (46 mg, 33%). mp 190–192 °C; HPLC purity: 17.74 min, 95.2%. <sup>1</sup>H NMR (600 MHz, CDCl<sub>3</sub>)  $\delta$  8.12 (d,  $J$  = 7.8 Hz, 2H), 8.05 (s, 1H), 7.68 (d,  $J$  = 8.4 Hz, 2H), 7.51 (dd,  $J$  = 7.1, 8.0 Hz, 2H), 7.47 (d,  $J$  = 7.1 Hz, 1H), 7.37 (d,  $J$  = 8.0 Hz, 2H), 2.48 (s, 3H). <sup>13</sup>C NMR (150 MHz, CDCl<sub>3</sub>)  $\delta$  187.3, 183.5, 146.9, 138.2, 134.0, 131.1, 130.8, 130.1, 129.4, 129.3, 129.1, 126.7, 22.2. HRMS (ESI<sup>+</sup>): calcd for [M+H]<sup>+</sup> C<sub>17</sub>H<sub>14</sub>NOS<sup>+</sup>  $m/z$  280.0791; found 280.0795.

**(Z)-5-(2-Methoxybenzylidene)-2-(p-tolyl)thiazol-4(5H)-one (2)**

A yellow solid (57 mg, 37%). mp 166–168 °C; HPLC purity: 17.77 min, 98.8%. <sup>1</sup>H NMR (600 MHz, DMSO-*d*<sub>6</sub>) δ 8.23 (s, 1H), 8.11 (d, *J* = 8.2 Hz, 2H), 7.69 (dd, *J* = 1.2, 7.7 Hz, 1H), 7.55 (ddd, *J* = 1.5, 8.6, 8.6 Hz, 1H), 7.48 (d, *J* = 8.2 Hz, 2H), 7.20 (d, *J* = 8.4 Hz, 1H), 7.16 (dd, *J* = 7.5, 7.6 Hz, 1H), 3.94 (s, 3H), 2.45 (s, 3H). <sup>13</sup>C NMR (150 MHz, DMSO-*d*<sub>6</sub>) δ 187.4, 182.2, 158.7, 146.8, 133.4, 131.7, 130.2, 129.1, 128.6, 128.6, 126.1, 121.9, 121.1, 112.1, 56.0, 21.5. HRMS (ESI<sup>+</sup>): calcd for [M+H]<sup>+</sup> C<sub>18</sub>H<sub>16</sub>NO<sub>2</sub>S<sup>+</sup> *m/z* 310.0896; found 310.0893.

**(Z)-5-(3-Methoxybenzylidene)-2-(p-tolyl)thiazol-4(5H)-one (3)**

A yellow solid (66 mg, 43%). mp 158–160 °C; HPLC purity: 17.94 min, 98.1%. <sup>1</sup>H NMR (600 MHz, CDCl<sub>3</sub>) δ 8.12 (d, *J* = 8.2 Hz, 2H), 8.01 (s, 1H), 7.42 (dd, *J* = 7.8, 8.2 Hz, 1H), 7.37 (d, *J* = 8.2 Hz, 2H), 7.28 (d, *J* = 7.8 Hz, 1H), 7.19 (d, *J* = 2.4 Hz, 1H), 7.02 (dd, *J* = 2.4, 8.2 Hz, 1H), 3.89 (s, 3H), 2.48 (s, 3H). <sup>13</sup>C NMR (150 MHz, CDCl<sub>3</sub>) δ 187.3, 183.5, 160.2, 146.9, 138.1, 135.4, 130.4, 130.1, 129.3, 129.1, 127.0, 123.4, 116.9, 115.8, 55.6, 22.2. ESIMS *m/z*: 310.0 [M + H]<sup>+</sup>. HRMS (ESI<sup>+</sup>): calcd for [M+H]<sup>+</sup> C<sub>18</sub>H<sub>16</sub>NO<sub>2</sub>S<sup>+</sup> *m/z* 310.0896; found 310.0890.

**(Z)-5-(4-Methoxybenzylidene)-2-(p-tolyl)thiazol-4(5H)-one (4)**

An orange solid (53 mg, 34%). mp 221–223 °C; HPLC purity: 17.74 min, 95.4%. <sup>1</sup>H NMR (600 MHz, CDCl<sub>3</sub>) δ 8.11 (d, *J* = 8.2 Hz, 2H), 8.02 (s, 1H), 7.65 (d, *J* = 8.6 Hz, 2H), 7.36 (d, *J* = 8.0 Hz, 2H), 7.02 (d, *J* = 8.6 Hz, 2H), 3.89 (s, 3H), 2.48 (s, 3H). <sup>13</sup>C NMR (150 MHz, CDCl<sub>3</sub>) δ 186.6, 183.8, 162.1, 146.5, 138.3, 132.0, 130.1, 129.5, 129.0, 126.7, 123.9, 115.0, 55.7, 22.1. HRMS (ESI<sup>+</sup>): calcd for [M+H]<sup>+</sup> C<sub>18</sub>H<sub>16</sub>NO<sub>2</sub>S<sup>+</sup> *m/z* 310.0896; found 310.0893.

**(Z)-5-(3,4-Dihydroxybenzylidene)-2-(p-tolyl)thiazol-4(5H)-one (5)**

A dark red solid (34 mg, 22%). mp 256–258 °C; HPLC purity: 15.19 min, 96.4%. <sup>1</sup>H NMR (600 MHz, MeOD) δ 8.11 (d, *J* = 8.2 Hz, 2H), 7.91 (s, 1H), 7.45 (d, *J* = 8.2 Hz, 2H), 7.24 (d, *J* = 2.4 Hz, 1H), 7.18 (dd, *J* = 8.2, 2.4 Hz, 1H), 6.92 (d, *J* = 8.2 Hz, 1H), 2.48 (s, 3H). <sup>13</sup>C NMR (150 MHz, MeOD) δ 188.6, 185.1, 151.3, 148.2, 147.4, 141.2, 131.2, 130.4, 129.7, 126.9, 126.8, 123.1, 118.0, 117.1, 21.9. HRMS (ESI<sup>+</sup>): calcd for [M+H]<sup>+</sup> C<sub>17</sub>H<sub>14</sub>NO<sub>3</sub>S<sup>+</sup> *m/z* 312.0689; found 312.0686.

**(Z)-5-(4-Hydroxy-3-methoxybenzylidene)-2-(p-tolyl)thiazol-4(5H)-one (6)**

A red-orange solid (42 mg, 26%). mp 197–199 °C; HPLC purity: 16.26 min, 95.9%.

<sup>1</sup>H NMR (600 MHz, CDCl<sub>3</sub>) δ 8.10 (d, *J* = 8.0 Hz, 2H), 7.98 (s, 1H), 7.36 (d, *J* = 8.0 Hz, 2H), 7.29 (d, *J* = 8.2 Hz, 1H), 7.15 (d, *J* = 1.8 Hz, 1H), 7.04 (d, *J* = 8.2 Hz, 1H), 6.08 (brs, OH), 4.00 (s, 3H), 2.48 (s, 3H). <sup>13</sup>C NMR (150 MHz, CDCl<sub>3</sub>) δ 186.4, 183.7, 148.9, 147.1, 146.6, 138.7, 130.1, 129.5, 129.0, 126.6, 125.8, 123.8, 115.4, 112.8, 56.2, 22.1. ESIMS *m/z*: 326.0 [M + H]<sup>+</sup>. HRMS (ESI<sup>+</sup>): calcd for [M+H]<sup>+</sup> C<sub>18</sub>H<sub>16</sub>NO<sub>3</sub>S<sup>+</sup> *m/z* 326.0845; found 326.0846.

**(Z)-5-(3,5-dimethoxybenzylidene)-2-(p-tolyl)thiazol-4(5H)-one (7)**

A yellow solid (64 mg, 38%). mp 184–186 °C; HPLC purity: 18.18 min, 91.7%. <sup>1</sup>H

NMR (600 MHz, CDCl<sub>3</sub>) δ 8.10 (d, *J* = 8.2 Hz, 2H), 7.94 (s, 1H), 7.36 (d, *J* = 8.2 Hz, 2H), 6.80 (d, *J* = 2.1 Hz, 1H), 6.80 (d, *J* = 2.1 Hz, 1H), 6.56 (dd, *J* = 2.1 Hz, 1H), 3.86 (s, 6H), 2.47 (s, 3H). <sup>13</sup>C NMR (150 MHz, CDCl<sub>3</sub>) δ 187.3, 183.4, 161.3, 146.9, 138.2, 135.8, 130.1, 129.3, 129.1, 127.2, 108.6, 103.2, 55.7, 22.1. ESIMS *m/z*: 340.0 [M + H]<sup>+</sup>. HRMS (ESI<sup>+</sup>): calcd for [M+H]<sup>+</sup> C<sub>19</sub>H<sub>18</sub>NO<sub>3</sub>S<sup>+</sup> *m/z* 340.1002; found 340.1008.

**(Z)-5-(3,4-Dimethoxybenzylidene)-2-(p-tolyl)thiazol-4(5H)-one (8)**

A yellow-orange solid (44 mg, 26%). mp 187–189 °C; HPLC purity: 17.08 min,

95.7%. <sup>1</sup>H NMR (600 MHz, CDCl<sub>3</sub>) δ 8.11 (d, *J* = 8.1 Hz, 2H), 8.00 (s, 1H), 7.36 (d, *J* = 8.1 Hz, 2H), 7.32 (dd, *J* = 1.7, 8.4 Hz, 1H), 7.18 (d, *J* = 1.7 Hz, 1H), 6.99 (d, *J* = 8.4 Hz, 1H), 3.99 (s, 3H), 3.97 (s, 3H), 2.48 (s, 3H). <sup>13</sup>C NMR (150 MHz, CDCl<sub>3</sub>) δ 186.4, 183.7, 150.9, 149.6, 146.6, 138.6, 130.1, 129.5, 129.0, 127.0, 125.6, 124.1, 112.9, 111.6, 56.3, 56.2, 22.2. ESIMS *m/z*: 340.0 [M + H]<sup>+</sup>. HRMS (ESI<sup>+</sup>): calcd for [M+H]<sup>+</sup> C<sub>19</sub>H<sub>18</sub>NO<sub>3</sub>S<sup>+</sup> *m/z* 340.1002; found 340.1004.

**(Z)-5-(3-Hydroxy-4,5-dimethoxybenzylidene)-2-(p-tolyl)thiazol-4(5H)-one (10)**

An orange solid (59 mg, 33%). mp 179–181 °C; HPLC purity: 16.33 min, 96.0%. <sup>1</sup>H

NMR (600 MHz, CDCl<sub>3</sub>) δ 8.10 (d, *J* = 8.2 Hz, 2H), 7.91 (s, 1H), 7.36 (d, *J* = 8.2 Hz, 2H), 7.00 (d, *J* = 1.9 Hz, 1H), 6.77 (d, *J* = 1.9 Hz, 1H), 5.97 (brs, OH), 3.99 (s, 3H), 3.94 (s, 3H), 2.48 (s, 3H). <sup>13</sup>C NMR (150 MHz, CDCl<sub>3</sub>) δ 187.0, 183.6, 152.6, 149.8, 146.8, 138.2, 138.1, 130.1, 129.8, 129.4, 129.1, 126.0, 110.1, 107.8, 61.3, 56.2, 22.1. HRMS (ESI<sup>+</sup>): calcd for [M+H]<sup>+</sup> C<sub>19</sub>H<sub>18</sub>NO<sub>4</sub>S<sup>+</sup> *m/z* 356.0951; found 356.0959.

**(Z)-5-(4-Hydroxy-3,5-dimethoxybenzylidene)-2-(p-tolyl)thiazol-4(5H)-one (11)**

A red-orange solid (50 mg, 28%). mp 227–229 °C; HPLC purity: 16.14 min, 98.5%.

<sup>1</sup>H NMR (600 MHz, CDCl<sub>3</sub>) δ 8.10 (d, *J* = 8.1 Hz, 2H), 7.96 (s, 1H), 7.36 (d, *J* = 8.1 Hz, 2H), 6.93 (s, 2H), 5.98 (brs, OH), 3.99 (s, 6H), 2.48 (s, 3H). <sup>13</sup>C NMR (150 MHz, CDCl<sub>3</sub>) δ 186.3, 183.6, 147.6, 146.6, 138.9, 138.2, 130.1, 129.4, 129.0, 125.6, 124.1, 108.1, 56.6, 22.2. HRMS (ESI<sup>+</sup>): calcd for [M+H]<sup>+</sup> C<sub>19</sub>H<sub>18</sub>NO<sub>4</sub>S<sup>+</sup> *m/z* 356.0951; found 356.0946.

**(Z)-5-(4-Isopropylbenzylidene)-2-(p-tolyl)thiazol-4(5H)-one (23)**

A yellow solid (59 mg, 37%). mp 146–148 °C; HPLC purity: 19.29 min, 91.0%. <sup>1</sup>H

NMR (600 MHz, CDCl<sub>3</sub>) δ 8.11 (d, *J* = 8.2 Hz, 2H), 8.04 (s, 1H), 7.62 (d, *J* = 8.2 Hz, 2H), 7.37 (m, 4H), 2.98 (m, 1H), 2.48 (s, 3H), 1.29 (d, *J* = 6.9 Hz, 6H). <sup>13</sup>C NMR (150 MHz, CDCl<sub>3</sub>) δ 187.0, 183.7, 152.8, 146.7, 138.4, 131.6, 131.1, 130.1, 129.4, 129.0, 127.6, 125.6, 34.4, 23.8, 22.1. HRMS (ESI<sup>+</sup>): calcd for [M+H]<sup>+</sup> C<sub>20</sub>H<sub>20</sub>NOS<sup>+</sup> *m/z* 322.1260; found 322.1268.

**(Z)-5-(4-(Dimethylamino)benzylidene)-2-(p-tolyl)thiazol-4(5H)-one (24)**

A purple solid (63 mg, 36%). mp 161–163 °C; HPLC purity: 18.00 min, 97.8%. <sup>1</sup>H

NMR (600 MHz, CDCl<sub>3</sub>) δ 8.10 (d, *J* = 8.4 Hz, 2H), 8.00 (s, 1H), 7.59 (d, *J* = 8.9 Hz, 2H), 7.33 (d, *J* = 8.2 Hz, 2H), 6.74 (d, *J* = 8.9 Hz, 2H), 3.10 (s, 6H), 2.46 (s, 3H), 1.22 (t, *J* = 7.2 Hz, 6H). <sup>13</sup>C NMR (150 MHz, CDCl<sub>3</sub>) δ 185.2, 184.1, 152.2, 145.8, 139.7, 133.4, 123.0, 129.8, 128.7, 121.6, 120.1, 112.1, 40.2, 22.0. HRMS (ESI<sup>+</sup>): calcd for [M+H]<sup>+</sup> C<sub>19</sub>H<sub>19</sub>N<sub>2</sub>OS<sup>+</sup> *m/z* 323.1213; found 323.1208.

**(Z)-5-(4-(Diethylamino)benzylidene)-2-(p-tolyl)thiazol-4(5H)-one (25)**

A purple solid (43 mg, 27%). mp 222–224 °C; HPLC purity: 18.79 min, 99.5%. <sup>1</sup>H

NMR (600 MHz, CDCl<sub>3</sub>) δ 8.09 (d, *J* = 8.0 Hz, 2H), 7.97 (s, 1H), 7.56 (d, *J* = 8.8 Hz, 2H), 7.33 (d, *J* = 8.0 Hz, 2H), 6.72 (d, *J* = 8.8 Hz, 2H), 3.44 (q, *J* = 7.1 Hz, 4H), 2.45 (s, 6H), 1.22 (t, *J* = 7.1 Hz, 6H). <sup>13</sup>C NMR (150 MHz, CDCl<sub>3</sub>) δ 184.9, 184.1, 150.1, 145.7, 139.7, 133.7, 129.9, 129.9, 128.6, 120.8, 119.4, 111.7, 44.8, 22.0, 12.7. HRMS (ESI<sup>+</sup>): calcd for [M+H]<sup>+</sup> C<sub>21</sub>H<sub>23</sub>N<sub>2</sub>OS<sup>+</sup> *m/z* 351.1526; found 351.1531.

**(Z)-5-(3,4-Dimethylbenzylidene)-2-(p-tolyl)thiazol-4(5H)-one (26)**

A yellow solid (38 mg, 25%). mp 200–202 °C; HPLC purity: 19.08 min, 92.1%. <sup>1</sup>H

NMR (600 MHz, CDCl<sub>3</sub>)  $\delta$  8.12 (d,  $J$  = 8.2 Hz, 2H), 8.01 (s, 1H), 7.44 (s, 1H), 7.43 (d,  $J$  = 6.4 Hz, 1H), 7.36 (d,  $J$  = 8.2 Hz, 2H), 7.26 (d,  $J$  = 6.4 Hz, 1H), 2.48 (s, 3H), 2.35 (s, 3H), 2.34 (s, 3H). <sup>13</sup>C NMR (150 MHz, CDCl<sub>3</sub>)  $\delta$  187.0, 183.7, 146.6, 140.9, 138.8, 137.8, 132.1, 131.7, 130.0, 130.1, 129.5, 129.0, 128.5, 125.3, 22.2, 20.2, 20.0. HRMS (ESI<sup>+</sup>): calcd for [M+H]<sup>+</sup> C<sub>19</sub>H<sub>18</sub>NOS<sup>+</sup>  $m/z$  308.1104; found 308.1100.

**(Z)-5-(4-Methylbenzylidene)-2-(*p*-tolyl)thiazol-4(5*H*)-one (27)**

A yellow solid (35 mg, 24%). mp 230–232 °C; HPLC purity: 18.47 min, 92.3%. <sup>1</sup>H NMR (600 MHz, CDCl<sub>3</sub>)  $\delta$  8.11 (d,  $J$  = 8.0 Hz, 2H), 8.03 (s, 1H), 7.58 (d,  $J$  = 7.8 Hz, 2H), 7.36 (d,  $J$  = 8.0 Hz, 2H), 7.31 (d,  $J$  = 7.8 Hz, 2H), 2.48 (s, 3H), 2.43 (s, 3H). <sup>13</sup>C NMR (150 MHz, CDCl<sub>3</sub>)  $\delta$  187.0, 183.7, 146.7, 142.0, 138.4, 131.3, 130.9, 130.2, 130.1, 129.4, 129.0, 125.5, 22.1, 21.8. HRMS (ESI<sup>+</sup>): calcd for [M+H]<sup>+</sup> C<sub>18</sub>H<sub>16</sub>N<sub>2</sub>OS<sup>+</sup>  $m/z$  294.0947; found 294.0950.

**(Z)-5-(3-Fluoro-4-methylbenzylidene)-2-(*p*-tolyl)thiazol-4(5*H*)-one (28)**

A yellow-orange solid (70 mg, 45%); HPLC purity: 18.60 min, 91.4%. mp 230–232 °C. <sup>1</sup>H NMR (600 MHz, CDCl<sub>3</sub>)  $\delta$  8.12 (d,  $J$  = 8.4 Hz, 2H), 7.97 (s, 1H), 7.38 (d,  $J$  = 8.4 Hz, 2H), 7.33 (m, 3H), 2.49 (s, 3H), 2.35 (d,  $J$  = 1.2 Hz, 3H). <sup>13</sup>C NMR (150 MHz, CDCl<sub>3</sub>)  $\delta$  187.0, 183.5, 161.7 (d,  $J$  = 247 Hz), 147.0, 136.9, 136.9, 133.6 (d,  $J$  = 7.8 Hz), 132.4 (d,  $J$  = 5.5 Hz), 130.2, 129.3, 129.2, 126.9 (d,  $J$  = 25.4 Hz), 126.8, 116.4 (d,  $J$  = 23.5 Hz), 22.8, 15.0. HRMS (ESI<sup>+</sup>): calcd for [M+H]<sup>+</sup> C<sub>18</sub>H<sub>15</sub>FNOS<sup>+</sup>  $m/z$  312.0853; found 312.0845.

**(Z)-5-(4-Fluoro-3-methylbenzylidene)-2-(*p*-tolyl)thiazol-4(5*H*)-one (29)**

A yellow solid (59 mg, 38%). mp 209–211 °C; HPLC purity: 18.47 min, 92.8%. <sup>1</sup>H NMR (600 MHz, CDCl<sub>3</sub>)  $\delta$  8.11 (d,  $J$  = 8.2 Hz, 2H), 7.97 (s, 1H), 7.51–7.50 (m, 2H), 7.37 (d,  $J$  = 8.2 Hz, 2H), 7.13 (dd,  $J$  = 9.1, 9.1 Hz, 1H), 2.48 (s, 3H), 2.37 (s, 3H). <sup>13</sup>C NMR (150 MHz, CDCl<sub>3</sub>)  $\delta$  187.0, 183.5, 162.9 (d,  $J$  = 254 Hz), 146.9, 137.3, 134.2 (d,  $J$  = 6.0 Hz), 130.3 (d,  $J$  = 5.7 Hz), 130.1, 130.1 (d,  $J$  = 3.7 Hz), 129.3, 129.1, 126.4 (d,  $J$  = 17.4 Hz), 126.0 (d,  $J$  = 2.5 Hz), 116.4 (d,  $J$  = 13.2 Hz), 22.2, 14.8 (d,  $J$  = 3.3 Hz). HRMS (ESI<sup>+</sup>): calcd for [M+H]<sup>+</sup> C<sub>18</sub>H<sub>15</sub>FNOS<sup>+</sup>  $m/z$  312.0853; found 312.0855.

**(Z)-2-(*p*-Tolyl)-5-(3-(trifluoromethyl)benzylidene)thiazol-4(5*H*)-one (30)**

An orange solid (59 mg, 34%). mp 196–198 °C; HPLC purity: 17.75 min, 93.2%. <sup>1</sup>H



NMR (600 MHz, CDCl<sub>3</sub>)  $\delta$  8.13 (d,  $J$  = 8.1 Hz, 2H), 8.03 (s, 1H), 7.90 (s, 1H), 7.84 (d,  $J$  = 7.7 Hz, 1H), 7.71 (d,  $J$  = 7.7 Hz, 1H), 7.64 (dd,  $J$  = 7.7, 7.7 Hz, 1H), 7.38 (d,  $J$  = 8.1 Hz, 2H), 2.49 (s, 3H). <sup>13</sup>C NMR (150 MHz, CDCl<sub>3</sub>)  $\delta$  187.2, 183.1, 147.3, 135.81, 134.9, 133.6, 132.0 (q,  $J$  = 32.8 Hz), 130.2, 130.0, 129.3, 129.1, 128.7, 127.3 (q,  $J$  = 3.8 Hz), 127.0 (q,  $J$  = 3.6 Hz), 123.8 (q,  $J$  = 273 Hz), 22.2. HRMS (ESI<sup>+</sup>): calcd for [M+H]<sup>+</sup> C<sub>18</sub>H<sub>13</sub>F<sub>3</sub>NOS<sup>+</sup>  $m/z$  348.0664; found 348.0674.

(*Z*)-5-(4-Chlorobenzylidene)-2-(*p*-tolyl)thiazol-4(5*H*)-one (**31**)

A brown solid (47 mg, 30%). mp 187–189 °C; HPLC purity: 17.78 min, 92.0%. <sup>1</sup>H NMR (600 MHz, CDCl<sub>3</sub>)  $\delta$  8.11 (d,  $J$  = 8.2 Hz, 2H), 7.98 (s, 1H), 7.61 (d,  $J$  = 8.5 Hz, 2H), 7.48 (d,  $J$  = 8.5 Hz, 2H), 7.37 (d,  $J$  = 8.2 Hz, 2H), 2.48 (s, 3H). <sup>13</sup>C NMR (150 MHz, CDCl<sub>3</sub>)  $\delta$  186.8, 183.2, 146.9, 137.0, 136.4, 132.4, 131.7, 130.1, 129.6, 129.1, 129.0, 127.1, 22.0. HRMS (ESI<sup>+</sup>): calcd for [M+H]<sup>+</sup> C<sub>17</sub>H<sub>13</sub>ClNOS<sup>+</sup>  $m/z$  314.0401; found 314.0398.

(*Z*)-5-(4-Bromobenzylidene)-2-(*p*-tolyl)thiazol-4(5*H*)-one (**32**)

A brown solid (64 mg, 36%). mp 240–242 °C; HPLC purity: 18.45 min, 93.5%. <sup>1</sup>H NMR (600 MHz, DMSO-*d*<sub>6</sub>)  $\delta$  8.12 (d,  $J$  = 7.7 Hz, 2H), 8.01 (s, 1H), 7.80 (d,  $J$  = 8.1 Hz, 2H), 7.76 (d,  $J$  = 8.1 Hz, 2H), 7.50 (d,  $J$  = 7.7 Hz, 2H), 2.46 (s, 3H). <sup>13</sup>C NMR (150 MHz, DMSO-*d*<sub>6</sub>)  $\delta$  186.3, 182.1, 147.0, 136.1, 132.7, 132.5, 132.3, 130.3, 128.7, 128.4, 127.2, 124.9, 21.5. HRMS (ESI<sup>+</sup>): calcd for [M+H]<sup>+</sup> C<sub>17</sub>H<sub>13</sub>BrNOS<sup>+</sup>  $m/z$  357.9896; found 357.9893.

(*Z*)-5-(2-Fluorobenzylidene)-2-(*p*-tolyl)thiazol-4(5*H*)-one (**33**)

A yellow solid (45 mg, 30%). mp 192–194 °C; HPLC purity: 18.61 min, 93.7%. <sup>1</sup>H NMR (600 MHz, CDCl<sub>3</sub>)  $\delta$  8.29 (s, 1H), 8.11 (d,  $J$  = 7.8 Hz, 2H), 7.74 (t,  $J$  = 7.2 Hz, 1H), 7.49–7.43 (m, 1H), 7.37 (d,  $J$  = 7.8 Hz, 2H), 7.30 (t,  $J$  = 7.2 Hz, 1H), 7.21–7.16 (m, 1H), 2.48 (s, 3H). <sup>13</sup>C NMR (150 MHz, CDCl<sub>3</sub>)  $\delta$  187.2, 183.1, 162.0 (d,  $J$  = 256.3 Hz), 147.0, 132.9 (d,  $J$  = 8.8 Hz), 130.2, 129.7 (d,  $J$  = 6.5 Hz), 129.4, 129.2, 129.1, 128.6, 124.8 (d,  $J$  = 4.7 Hz), 122.5 (d,  $J$  = 11.7 Hz), 116.4 (d,  $J$  = 21.7 Hz), 22.0. HRMS (ESI<sup>+</sup>): calcd for [M+H]<sup>+</sup> C<sub>17</sub>H<sub>13</sub>FNOS<sup>+</sup>  $m/z$  298.0696; found 298.0690.

(*Z*)-5-(4-Fluorobenzylidene)-2-(*p*-tolyl)thiazol-4(5*H*)-one (**34**)

A yellow solid (42 mg, 28%). mp 226–228 °C; HPLC purity: 17.43 min, 93.8%. <sup>1</sup>H



NMR (600 MHz, CDCl<sub>3</sub>)  $\delta$  8.11 (d,  $J = 8.2$  Hz, 2H), 8.01 (s, 1H), 7.68 (dd,  $J = 5.3$ , 8.5 Hz, 2H), 7.37 (d,  $J = 8.2$  Hz, 2H), 7.20 (t,  $J = 8.5$ , 8.5 Hz, 2H), 2.48 (s, 3H). <sup>13</sup>C NMR (150 MHz, CDCl<sub>3</sub>)  $\delta$  186.9, 183.3, 164.1 (d,  $J = 255$  Hz), 146.8, 136.7, 132.8 (d,  $J = 8.7$  Hz), 130.4 (d,  $J = 3.3$  Hz), 130.2, 129.3, 129.1, 126.4 (d,  $J = 2.6$  Hz), 116.7 (d,  $J = 22.1$  Hz), 22.0. HRMS (ESI<sup>+</sup>): calcd for [M+H]<sup>+</sup> C<sub>17</sub>H<sub>13</sub>FNOS<sup>+</sup>  $m/z$  298.0696; found 298.0689.

(Z)-5-(2,4-Difluorobenzylidene)-2-(*p*-tolyl)thiazol-4(5*H*)-one (**35**)

A yellow solid (55 mg, 35%). mp 196–198 °C; HPLC purity: 17.57 min, 93.6%. <sup>1</sup>H NMR (600 MHz, CDCl<sub>3</sub>)  $\delta$  8.20 (s, 1H), 8.10 (d,  $J = 8.2$  Hz, 2H), 7.75-7.71 (m, 1H), 7.37 (d,  $J = 8.2$  Hz, 2H), 7.06-7.03 (m, 1H), 6.96-6.92 (m, 1H), 2.48 (s, 3H). <sup>13</sup>C NMR (150 MHz, CDCl<sub>3</sub>)  $\delta$  186.9, 183.0, 163.5 (dd,  $J = 12.2$ , 255 Hz), 162.5 (dd,  $J = 12.0$ , 255 Hz), 147.2, 130.6 (dd,  $J = 3.0$ , 10.0 Hz), 130.2, 129.2, 129.2, 128.4 (dd,  $J = 1.7$ , 6.0 Hz), 128.2, 119.1 (dd,  $J = 3.9$ , 12.0, Hz), 112.3 (dd,  $J = 3.7$ , 21.8 Hz), 105.1 (dd,  $J = 25.5$ , 25.5 Hz), 22.2. HRMS (ESI<sup>+</sup>): calcd for [M+H]<sup>+</sup> C<sub>17</sub>H<sub>12</sub>F<sub>2</sub>NOS<sup>+</sup>  $m/z$  316.0602; found 316.0607.

(Z)-5-(4-(Benzyloxy)benzylidene)-2-(*p*-tolyl)thiazol-4(5*H*)-one (**36**)

An orange solid (66 mg, 34%). mp 182–184 °C; HPLC purity: 17.71 min, 95.6%. <sup>1</sup>H NMR (600 MHz, CDCl<sub>3</sub>)  $\delta$  8.11 (d,  $J = 8.2$  Hz, 2H), 8.01 (s, 1H), 7.64 (d,  $J = 8.3$  Hz, 2H), 7.45-7.40 (m, 4H), 7.41 (d,  $J = 7.8$  Hz, 2H), 7.37-7.35 (m, 3H), 7.09 (d,  $J = 8.8$  Hz, 2H), 5.15 (s, 2H), 2.47 (s, 3H). <sup>13</sup>C NMR (150 MHz, CDCl<sub>3</sub>)  $\delta$  186.6, 183.8, 161.2, 146.5, 138.2, 136.2, 132.9, 130.1, 129.5, 129.0, 128.9, 128.5, 127.6, 126.9, 124.0, 115.8, 70.4, 22.1. HRMS (ESI<sup>+</sup>): calcd for [M+H]<sup>+</sup> C<sub>24</sub>H<sub>20</sub>NO<sub>2</sub>S<sup>+</sup>  $m/z$  386.1209; found 386.1211.

(Z)-Methyl 4-((4-oxo-2-(*p*-tolyl)thiazol-5(4*H*)-ylidene)methyl)benzoate (**37**)

A yellow-orange solid (49 mg, 29%). mp 212–214 °C; HPLC purity: 18.94 min, 95.1%. <sup>1</sup>H NMR (600 MHz, CDCl<sub>3</sub>)  $\delta$  8.14 (d,  $J = 8.2$  Hz, 2H), 8.11 (d,  $J = 8.2$  Hz, 2H), 8.02 (s, 1H), 7.71 (d,  $J = 8.2$  Hz, 2H), 7.37 (d,  $J = 8.2$  Hz, 2H), 3.95 (s, 3H), 2.48 (s, 3H). <sup>13</sup>C NMR (150 MHz, CDCl<sub>3</sub>)  $\delta$  187.3, 183.2, 166.3, 147.3, 138.1, 136.3, 131.7, 130.4, 130.4, 130.2, 129.2, 129.1, 129.0, 52.6, 22.2. HRMS (ESI<sup>+</sup>): calcd for [M+H]<sup>+</sup> C<sub>19</sub>H<sub>16</sub>NOS<sup>+</sup>  $m/z$  338.0845; found 338.0847.

### ***In vitro* Enzymatic Assay**

The *in vitro* enzymatic assay against PRMT5 was carried out by Shanghai ChemPartner Co. (998 Halei Road, Pudong New District, Shanghai 201203, China). All of the inhibitory rate data were obtained by performing triplicate tests and showed as the mean value. IC<sub>50</sub> values were tested with eight different concentrations (from 100  $\mu$ M, 3 times dilution) of each compound and showed as the mean  $\pm$  SD of three replicates. The following materials were purchased: PRMT5/MEP50 (BPS, Cat. No. 51045); PRMT1 (BPS, Cat. No. 51041); [<sup>3</sup>H]-SAM (PerkinElmer, Lot. No. 2146246); SAM (Sigma, Cat. No. A7007); SAH (Sigma, Cat. No. A9384-25MG); 384-well plate (Perkin Elmer, Cat. No. 6007299); Anti-methyl-H4R3 AlphaLISA acceptor beads, streptavidin-tagged donor beads (Perkin Elmer); 1 x Epigenetics Buffer (Perkin Elmer). SAH was used as the reference compound. All tested compounds were dissolved into 20 mM stock in 100% DMSO. AlphaLISA and radioactive methylation assays were used to test the inhibitory activities against PRMT5 and PRMT1, respectively, following the method we previously reported.<sup>15</sup> The following protocol was used to test the inhibitory activity against PRMT5. Briefly, the biotinylated unmethylated histone H4 peptide (the 23-amino acid sequence: SGRGKGGKGLGKGGAKRHRKVLGGK(biotin) - NH<sub>2</sub>) substrate at arginine 3 (unmeH4R3) substrate stock and the SAM stock was diluted using Assay buffer (10mM Tris, PH 8.0, 1mM DTT, 0.01% Tween-20) with final concentrations of 50 nM and 64  $\mu$  M respectively in the reaction well. The PRMT5/MEP50 enzyme was diluted at a ratio of 1 : 10 in Assay buffer before being used. 100 nL of compound solutions were transferred to each well of the assay plate. Next, 5  $\mu$ L of unmeH4R3:SAM mixture and 5  $\mu$ L of diluted enzyme stock (final concentration of 0.25 nM) were mixed in each well and incubated at room temperature (RT) for 60 min. 10  $\mu$ L of the assay buffer was used to serve as positive “maximum signal” control (no compound, with PRMT5 enzyme added), while “background signal” control was with no compound and no enzyme added. After that, 7.5  $\mu$ L anti-H4R3me<sub>2</sub> acceptor beads (1 : 300 dilution of the 5 mg/ml stock in 1 x Epigenetics buffer) and 7.5  $\mu$ L

streptavidin-coated donor bead beads (1 : 300 dilution of the 5 mg/mL stock in 1x Epigenetics buffer) were successively added to each well of the assay plates with an interval of 60 min. The plates were incubated at RT for 30 min in the dark followed by Alpha signal reading on an EnSpire reader. GraphPad Prism 5.0 was used to process data.

The following protocol was used to test the inhibitory activity of compound **5** against PRMT1. The enzyme (PRMT1), substrate (H4R3 S1ac), [<sup>3</sup>H]-SAM and Stop Mix (SAM) solution were prepared in assay buffer with the final concentration of 0.5 nM, 0.1 μM, 0.25 μM and 0.13 mM, respectively. Compounds were added to the assay plate by Echo. 15 μL Enzyme solution was added to per well of prepared compound stock plates, followed by addition of 10 μL peptide and [<sup>3</sup>H]-SAM to per well of prepared compound stock plate using Multidrop. The plates were then covered and incubated for 60 minutes at room temperature. The reaction was finally stopped by addition of 5 μL Stop Mix. 25 μL solution from per well of the compound stock plate was transferred to Flashplate using Platemate, and the Flashplate was covered and then incubated for another 60 min at room temperature. The Flashplate was washed with dH<sub>2</sub>O + 0.1% Tween using the BioTek plate washer and then read plate in TopCount using program 3H-flashplate.

### **Molecular dynamics simulation**

100 ns MD simulations were performed on **5**-PRMT5:MEP50 and **19**-PRMT5:MEP50 complex models obtained by molecular docking. H++ program<sup>26</sup> was used to predict the protonation states of ionizable residues of each model. A periodic box of transferable intermolecular potential 3P water molecules that extended 10.0 Å from the protein atoms was performed on each complex model. In order to neutralize the simulation system, counterions were added. AMBER 14.0 package<sup>27</sup> was used to perform MD simulations. Each model was done with isothermal-isobaric (NPT) ensemble and periodic boundary conditions. The force field for protein and small molecules were Amber14SB and the general Amber force field (GAFF)<sup>28</sup> respectively. Antechamber<sup>29</sup> was used to derive charges and force field parameters of small molecules that were not existent in GAFF. SHAKE algorithm<sup>30</sup> and

particle-mesh Ewald method<sup>31</sup> were respectively used to constrain small bonds involving hydrogen atoms and to calculate the electrostatic interactions. The non-bonded pairs were updated every 25 steps while the non-bonded cutoff was set to 10 Å. Each MD simulation was coupled to a 300 K thermal bath at 1 bar pressure by using the algorithm of Berendsen et al.<sup>32</sup>

#### **MM/PBSA calculations.**

After the trajectory of each complex model was well equilibrated, binding free energy was calculated using the MM/PBSA method encoded in the AMBER 14.0 program. 2000 snapshots from each model trajectory were extracted every 50 ps, and the MM/PBSA calculation was performed on each snapshot using the MMPBSA.py.MPI module.

#### ***In vitro* anti-proliferative assay on MV4-11 cell line.**

Cell viability was measured by the method described previously.<sup>15</sup> Briefly, MV4-11 cells were plated into 24-well plates with 1 mL of RPMI1640 medium (Invitrogen) containing 10% fetal bovine serum and 1% penicillin/streptomycin at a density of  $0.5-1 \times 10^5$  cells per well. The cells were incubated with tested compounds at different concentrations or DMSO at 37 °C in an incubator with a supply of 5% CO<sub>2</sub> for four, eight, and 12 days. Viable cell number was determined using the Cell Titer-Glo Luminescent Cell Viability assays (Promega), and luminescence was recorded using an EnVision Multilabel Plate Readers (PerkinElmer) according to the manufacturer's protocol. EC<sub>50</sub> values were determined from at least three independent tests and calculated from the inhibition curves.

#### **Western Blotting**

Total cell lysates were separated by 4%–12% SDS-polyacrylamide gels and transferred to nitrocellulose membranes. Then blocking buffer (5% nonfat milk in PBST) and primary antibodies (SDMA, CST, 13222s; GAPDH, CST, 5174; both prepared in a 1:3 dilution of blocking buffer) were subsequently used to block and

incubate the blots for one hour at room temperature and overnight at 4 °C, respectively. After being washed three times with PBST, the blots were incubated with 1:10000 dilution of donkey anti-rabbit secondary antibody (HRP conjugated) for one hour. Finally, the bands were detected in the ChemiScope3400 imaging system using ECL substrate (Millipore).

### Flow Cytometric Analysis

MV4-11 cells were plated in 6-well plates and treated with tested compounds (**5** and **19**) or DMSO (control). For cell cycle analysis, cells harvested after 24 hours were re-suspended in 70% ethanol overnight at 4 °C for fixation. After washed with PBS, samples were incubated with Propidium Iodide/RNase Staining Buffer (BD Pharmingen) for 30 minutes at room temperature. For cell apoptosis analysis, cells harvested after 48 hours were measured using AnnexinV-FITC Apoptosis Detection Kit (Vazyme Biotech) according to the manufacturer's protocol. Samples were detected by BD FACSCalibur (BD Pharmingen) and data were analyzed using FlowJo V7.6.1.

### Conclusions

In conclusion, 11 novel PRMT5 inhibitors were identified with IC<sub>50</sub> values ranging from 0.77 to 23 μM by docking-based virtual screening combined with biological evaluation. Compared with the previously reported PRMT5 inhibitors, the hits identified in this work contained a new scaffold and could be used for further optimization to improve their activities. From the proposed binding mode, the top two active hits (**5** and **19**) had hydrophobic, hydrogen bond, salt bridge and cation-π interactions with PRMT5. MD simulation results indicated that the order of the binding free energy was in well agreement with the experimental activity. In addition, the anti-proliferative effect and the cell-level target engagement of **5** and **19** were confirmed in MV4-11 cells. Further investigations uncovered the G1 cell-cycle arrest and inducement of cell apoptosis to be the mechanism of cellular activity. The hits discovered in this study has provided a new chemical template for further hit-to-lead

optimization and lay a foundation for further development of therapeutic candidates for cancer.

### Abbreviations

PRMT, protein arginine methyltransferase; SAM, sadenosylmethionine; MEP50, methylosome protein 50; MD, molecular dynamics; MM/PBSA, Molecular mechanics/Poisson-Boltzmann surface area; SAR, structure-activity relationship.

### Acknowledgements

This work was supported by the Shandong Provincial Natural Science Foundation [Nos. ZR2017BH038, JQ201721], National Natural Science Foundation of China [Nos. 21672082, 21472208, 81625022, and 81430084], Shandong Key Development Project [No. 2016GSF201209], the Young Taishan Scholars Program [No. tsqn20161037], Shandong Talents Team Cultivation Plan of University Preponderant Discipline [No. 10027], and China Postdoctoral Science Foundation [2016M590391].

### Reference

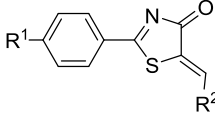
1. V. Karkhanis, Y. J. Hu, R. A. Baiocchi, A. N. Imbalzano and S. Sif, *Trends Biochem. Sci.*, 2011, **36**, 633-641.
2. E. S. Burgos, C. Wilczek, T. Onikubo, J. B. Bonanno, J. Jansong, U. Reimer and D. Shechter, *J. Biol. Chem.*, 2015, **290**, 9674-9689.
3. Q. Zhao, G. Rank, Y. T. Tan, H. Li, R. L. Moritz, R. J. Simpson, L. Cerruti, D. J. Curtis, D. J. Patel, C. D. Allis, J. M. Cunningham and S. M. Jane, *Nat. Struct. Mol. Biol.*, 2009, **16**, 304-311.
4. S. Pal, S. N. Vishwanath, H. Erdjument-Bromage, P. Tempst and S. Sif, *Mol. Cell Biol.*, 2004, **24**, 9630-9645.
5. E. Chan-Penebre, K. G. Kuplast, C. R. Majer, P. A. Boriack-Sjodin, T. J. Wigle, L. D. Johnston, N. Rioux, M. J. Munchhof, L. Jin, S. L. Jacques, K. A. West, T. Lingaraj, K. Stickland, S. A. Ribich, A. Raimondi, M. P. Scott, N. J. Waters, R. M. Pollock, J. J. Smith, O. Barbash, M. Pappalardi, T. F. Ho, K. Nurse, K. P. Oza, K. T. Gallagher, R. Kruger, M. P. Moyer, R. A. Copeland, R. Chesworth and K. W. Duncan, *Nat. Chem. Biol.*, 2015, **11**, 432-437.
6. X. Sheng and Z. Wang, *BMC Cancer*, 2016, **16**, 567.
7. F. Yan, L. Alinari, M. E. Lustberg, L. K. Martin, H. M. Cordero-Nieves, Y. Banasavadi-Siddegowda, S. Virk, J. Barnholtz-Sloan, E. H. Bell, J. Wojton, N. K. Jacob, A. Chakravarti, M. O. Nowicki, X. Wu, R. Lapalombella, J. Datta, B.

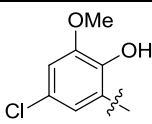
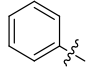
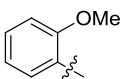
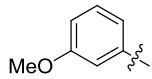
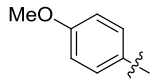
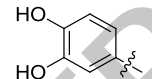
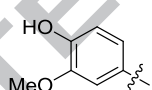
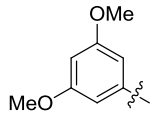
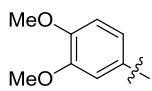
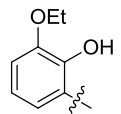
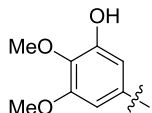
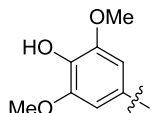
- Yu, K. Gordon, A. Haseley, J. T. Patton, P. L. Smith, J. Ryu, X. Zhang, X. Mo, G. Marcucci, G. Nuovo, C. H. Kwon, J. C. Byrd, E. A. Chiocca, C. Li, S. Sif, S. Jacob, S. Lawler, B. Kaur and R. A. Baiocchi, *Cancer Res*, 2014, **74**, 1752-1765.
8. M. A. Powers, M. M. Fay, R. E. Factor, A. L. Welm and K. S. Ullman, *Cancer Res.*, 2011, **71**, 5579-5587.
  9. J. Chung, V. Karkhanis, S. Tae, F. Yan, P. Smith, L. W. Ayers, C. Agostinelli, S. Pileri, G. V. Denis, R. A. Baiocchi and S. Sif, *J. Biol. Chem.*, 2013, **288**, 35534-35547.
  10. L. Wang, S. Pal and S. Sif, *Mol. Cell. Biol.*, 2008, **28**, 6262-6277.
  11. S. Pal, R. A. Baiocchi, J. C. Byrd, M. R. Grever, S. T. Jacob and S. Sif, *EMBO J.*, 2007, **26**, 3558-3569.
  12. F. Ye, W. Zhang, X. Ye, J. Jin, Z. Lv and C. Luo, *J. Chem. Inf. Model.*, 2018, **58**, 1066-1073.
  13. S. Antonysamy, Z. Bonday, R. M. Campbell, B. Doyle, Z. Druzina, T. Gheyi, B. Han, L. N. Jungheim, Y. W. Qian, C. Rauch, M. Russell, J. M. Sauder, S. R. Wasserman, K. Weichert, F. S. Willard, A. P. Zhang and S. Emtage, *P. Natl. Acad. Sci. USA.*, 2012, **109**, 17960-17965.
  14. Y. Ye, B. Zhang, R. Mao, C. Zhang, Y. Wang, J. Xing, Y. C. Liu, X. Luo, H. Ding, Y. Yang, B. Zhou, H. Jiang, K. Chen, C. Luo and M. Zheng, *Org. Biomol. Chem.*, 2017, **15**, 3648-3661.
  15. R. Mao, J. Shao, K. Zhu, Y. Zhang, H. Ding, C. Zhang, Z. Shi, H. Jiang, D. Sun, W. Duan and C. Luo, *J. Med. Chem.*, 2017, **60**, 6289-6304.
  16. S. Ji, S. Ma, W. J. Wang, S. Z. Huang, T. Q. Wang, R. Xiang, Y. G. Hu, Q. Chen, L. L. Li and S. Y. Yang, *Chem. Biol. Drug Des.*, 2017, **89**, 585-598.
  17. G. B. Gonsalvez, L. Tian, J. K. Ospina, F. M. Boisvert, A. I. Lamond and A. G. Matera, *J. Cell Biol.*, 2007, **178**, 733-740.
  18. W. J. Friesen, S. Paushkin, A. Wyce, S. Massenet, G. S. Pesiridis, G. Van Duyne, J. Rappsilber, M. Mann and G. Dreyfuss, *Mol. Cell Biol.*, 2001, **21**, 8289-8300.
  19. G. Meister, C. Eggert, D. Buhler, H. Brahm, C. Kambach and U. Fischer, *Curr. Biol.*, 2001, **11**, 1990-1994.
  20. K. W. Duncan, N. Rioux, P. A. Boriack-Sjodin, M. J. Munchhof, L. A. Reiter, C. R. Majer, L. Jin, L. D. Johnston, E. Chan-Penebre, K. G. Kuplast, M. P. Scott, R. M. Pollock, N. J. Waters, J. J. Smith, M. P. Moyer, R. A. Copeland and R. Chesworth, *ACS Med. Chem. Lett.*, 2016, **7**, 162-166.
  21. K. Mavrakis, E. R. McDonald, M. R. Schlabach, E. Billy, G. R. Hoffman, A. deWeck, D. A. Ruddy, K. Venkatesan, G. McAllister, R. deBeaumont, S. Ho, Y. Liu, Y. Yan-Neale, G. Z. Yang, F. Lin, H. Yin, H. Gao, D. R. Kipp, S. P. Zhao, J. T. McNamara, E. R. Sprague, Y. S. Cho, J. Gu, K. Crawford, V. Capka, K. Hurov, J. A. Porter, J. Tallarico, C. Mickanin, E. Lees, R. Pagliarini, N. Keen, T. Schmelzle, F. Hofmann, F. Stegmeier and W. R. Sellers, *Science*, 2016, **351**, 1208-1213.
  22. B. Hofmann, S. Barzen, C. B. Rodl, A. Kiehl, J. Borig, A. Zivkovic, H. Stark,

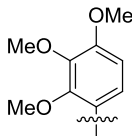
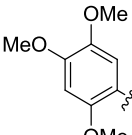
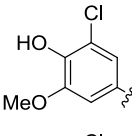
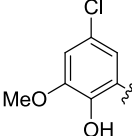
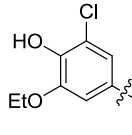
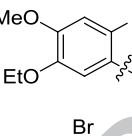
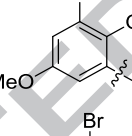
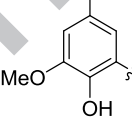
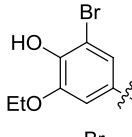
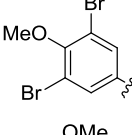
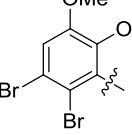
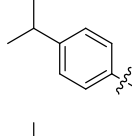
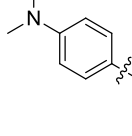


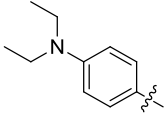
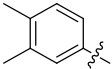
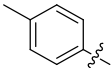
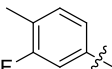
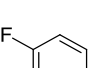
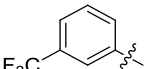
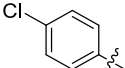
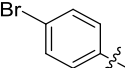
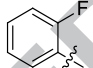
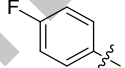
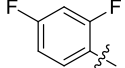
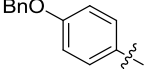
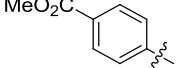
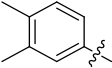
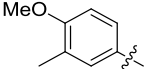
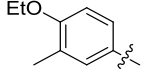
- G. Schneider and D. Steinhilber, *J. Med. Chem.*, 2011, **54**, 1943-1947.
23. Y. K. Banasavadi-Siddegowda, L. Russell, E. Frair, V. A. Karkhanis, T. Relation, J. Y. Yoo, J. Zhang, S. Sif, J. Imitola, R. Baiocchi and B. Kaur, *Oncogene*, 2017, **36**, 263-274.
24. T. A. Halgren, R. B. Murphy, R. A. Friesner, H. S. Beard, L. L. Frye, W. T. Pollard and J. L. Banks, *J. Med. Chem.*, 2004, **47**, 1750-1759.
25. R. A. Friesner, J. L. Banks, R. B. Murphy, T. A. Halgren, J. J. Klicic, D. T. Mainz, M. P. Repasky, E. H. Knoll, M. Shelley, J. K. Perry, D. E. Shaw, P. Francis and P. S. Shenkin, *J. Med. Chem.*, 2004, **47**, 1739-1749.
26. J. C. Gordon, J. B. Myers, T. Folta, V. Shoja, L. S. Heath and A. Onufriev, *Nucleic Acids Res.*, 2005, **33**, W368-371.
27. D. A. Case, T. E. Cheatham, 3rd, T. Darden, H. Gohlke, R. Luo, K. M. Merz, Jr., A. Onufriev, C. Simmerling, B. Wang and R. J. Woods, *J. Comput. Chem.*, 2005, **26**, 1668-1688.
28. J. Wang, R. M. Wolf, J. W. Caldwell, P. A. Kollman and D. A. Case, *J. Comput. Chem.*, 2004, **25**, 1157-1174.
29. J. Wang, W. Wang, P. A. Kollman and D. A. Case, *J. Mol. Graph. Model.*, 2006, **25**, 247-260.
30. J. P. Ryckaert, G. Ciccotti, H. J. C. Berendsen, *J. Comput. Phys.*, 1977, **23**, 327-341.
31. T. Darden, Y. Darrin, L. Pedersen, *J. Chem. Phys.* 1993, **98**, 10089-10092.
32. H. J. C. Berendsen, J. P. M. Postma, W. F. V. Gunsteren, A. Dinola, J. R. Haak, *J. Chem. Phys.*, 1984, **81**, 3684-3690.

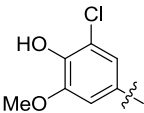
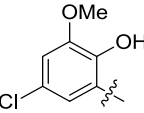
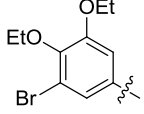
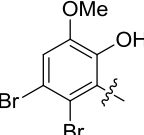


**Table 1** Inhibitory activity of **P16** and its analogues (**1** to **44**) against PRMT5<sup>a</sup>


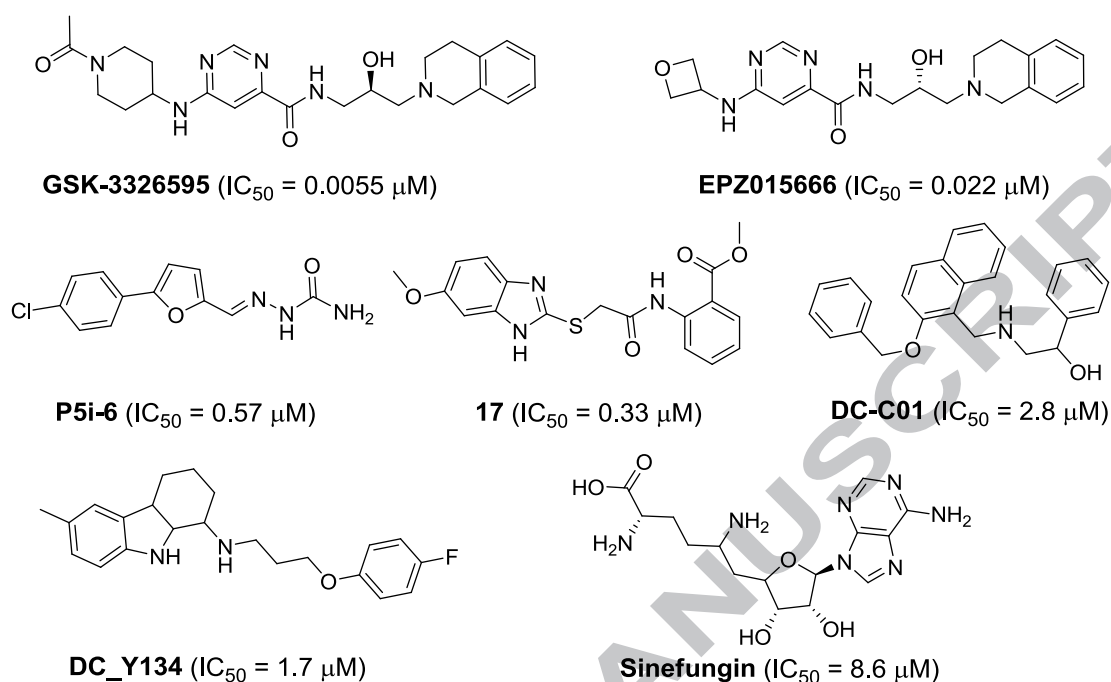
Compd. No.	R <sup>1</sup>	R <sup>2</sup>	Inhibition rate (%)	IC <sub>50</sub> (μM)	Source
<b>P16</b>	Me		62	13.9 ± 0.85	Specs
<b>1</b>	Me		5	N.D.	Synthesis
<b>2</b>	Me		9	N.D.	Synthesis
<b>3</b>	Me		12	N.D.	Synthesis
<b>4</b>	Me		33	N.D.	Synthesis
<b>5</b>	Me		82	0.77 ± 0.04	Synthesis
<b>6</b>	Me		24	N.D.	Synthesis
<b>7</b>	Me		15	N.D.	Synthesis
<b>8</b>	Me		7	N.D.	Synthesis
<b>9</b>	Me		6	N.D.	Specs
<b>10</b>	Me		20	N.D.	Synthesis
<b>11</b>	Me		18	N.D.	Synthesis

12	Me		30	N.D.	Specs
13	Me		27	N.D.	Specs
14	Me		56	$16 \pm 0.71$	Specs
15	Me		80	$12 \pm 1.41$	Specs
16	Me		44	$23 \pm 2.12$	Specs
17	Me		28	N.D.	Specs
18	Me		33	N.D.	Specs
19	Me		98	$6.6 \pm 0.50$	Specs
20	Me		42	$18 \pm 0.85$	Specs
21	Me		0	N.D.	Specs
22	Me		89	$16 \pm 0.14$	Specs
23	Me		30	N.D.	Synthesis
24	Me		4	N.D.	Synthesis

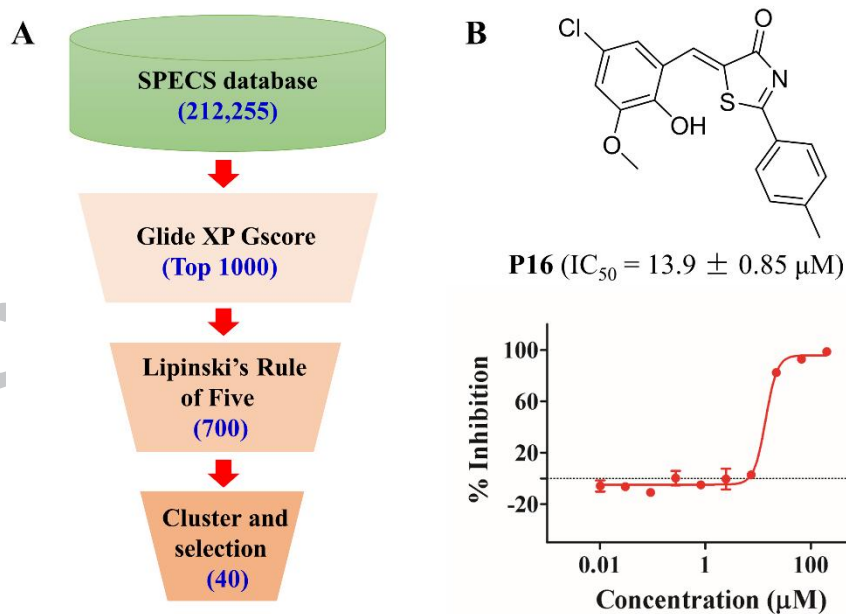
25	Me		0	N.D.	Synthesis
26	Me		14	N.D.	Synthesis
27	Me		4	N.D.	Synthesis
28	Me		14	N.D.	Synthesis
29	Me		0	N.D.	Synthesis
30	Me		30	N.D.	Synthesis
31	Me		14	N.D.	Synthesis
32	Me		0	N.D.	Synthesis
33	Me		25	N.D.	Synthesis
34	Me		2	N.D.	Synthesis
35	Me		17	N.D.	Synthesis
36	Me		17	N.D.	Synthesis
37	Me		0	N.D.	Synthesis
38	H		26	N.D.	Specs
39	H		8	N.D.	Specs
40	H		2	N.D.	Specs

41	H		48	$11 \pm 0.35$	Specs
42	H		65	$15 \pm 0.64$	Specs
43	H		23	N.D.	Specs
44	H		93	$17 \pm 0.28$	Specs

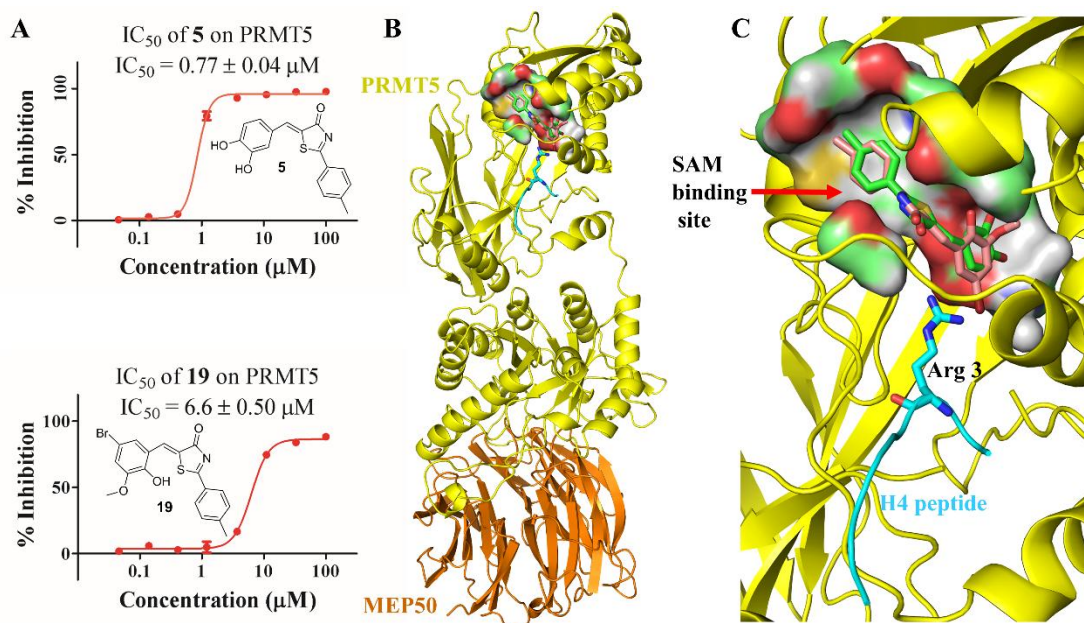
<sup>a</sup> The initial inhibition rates were tested at 50  $\mu$ M, and only compounds with >40% inhibition rates were selected for IC<sub>50</sub> measurements. N.D. = not determined. Data shown are mean  $\pm$  SD of three replicates.



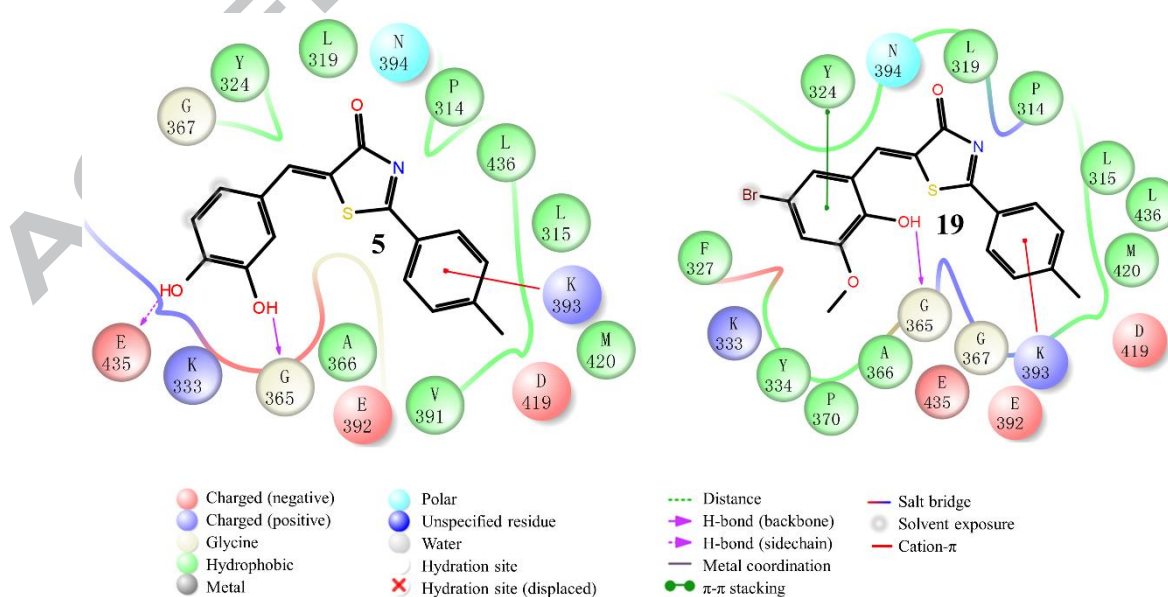
**Fig. 1** Previously reported PRMT5 inhibitors of six scaffolds.



**Fig. 2** Virtual screening procedures and activity assay results for PRMT5 in vitro. (A) Workflow of virtual screening. (B) Structure and inhibitory activity of **P16** against PRMT5 at enzymatic level.

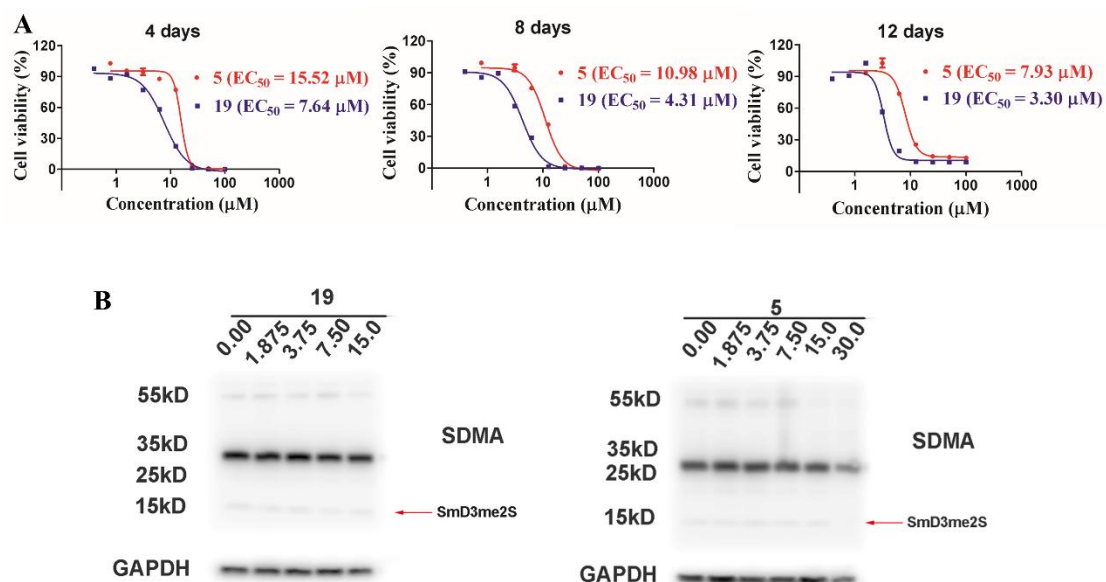


**Fig. 3** Chemical structures and inhibitory activities against PRMT5 of **5** and **19** and their predicted binding modes with PRMT5. (A) Structures and inhibition curves of compounds **5** and **19** against PRMT5. (B) Binding mode analysis of **5** and **19** with PRMT5. PRMT5, MEP50 and H4 peptide are shown in cartoon diagram in yellow, orange, and cyan color, respectively, and **5** and **19** are represented as green and salmon sticks, respectively. (C) A close-up view of the binding modes of **5** and **19**. Arginine 3 of H4 peptide is shown as cyan sticks.

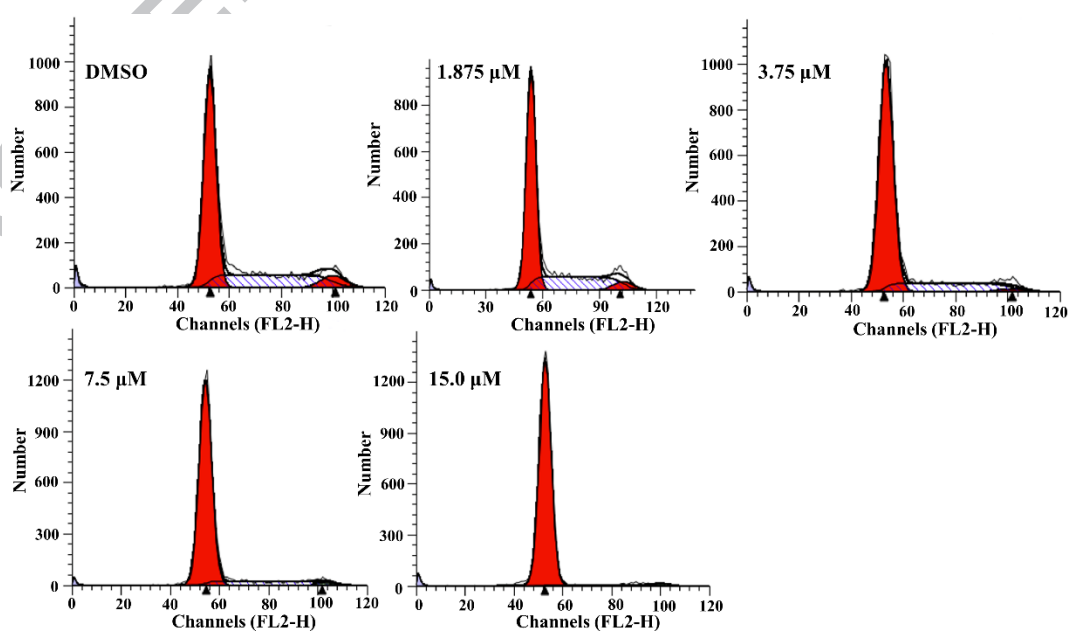


**Fig. 4** The detailed interactions of **5** and **19** with PRMT5 obtained by molecular

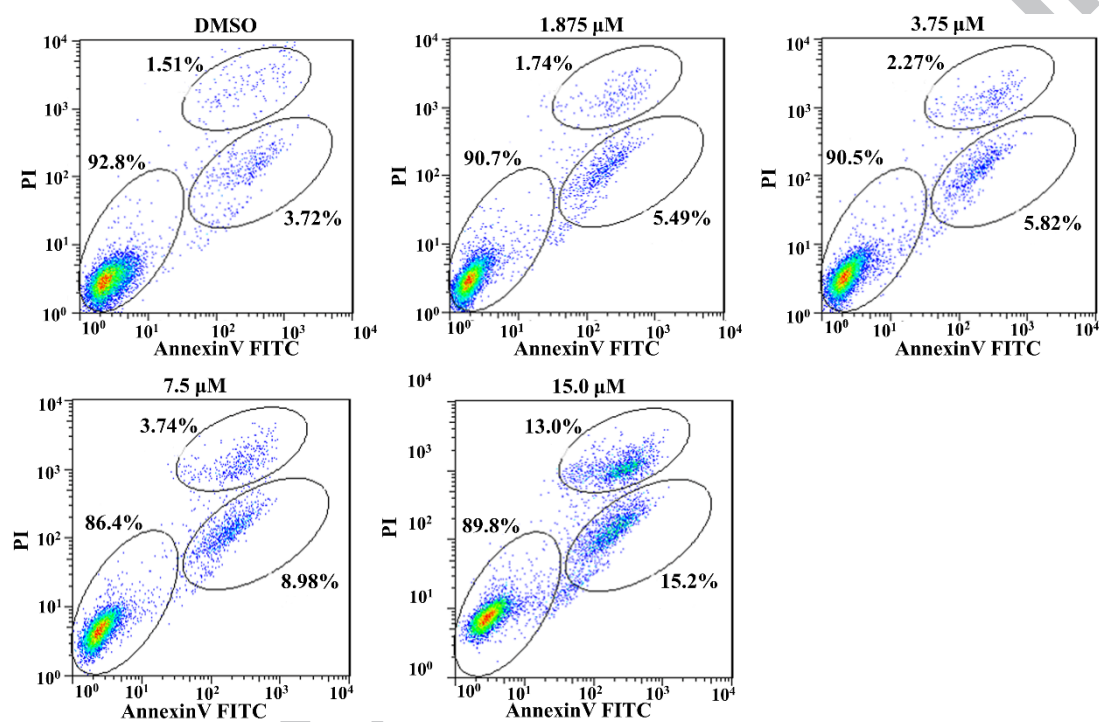
docking. The Lig. Int. panel inserted in Maestro was used to display ligand interaction diagram.



**Fig.5** Cell viability and Western blot analysis. (A) Effects of **5** and **19** on the proliferation of MV4-11 cells. (B) Effects of **19** and **5** on cellular target inhibition as determined by SDMA western blot. Treatment with **5** and **19** for 96 h decreased the cellular symmetrically dimethylation levels in MV4-11 cells.



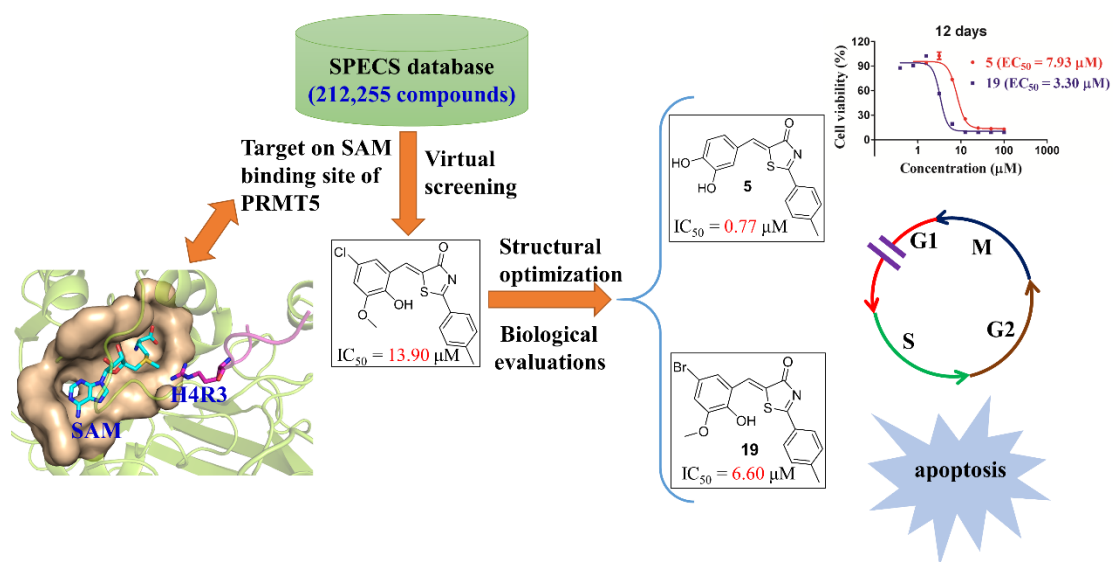
**Fig. 6** Cell cycle arrest in MV4-11 cells after treatment with **19**. Treatment with **19** arrested MV4-11 cells at G1 phase measured after 24 h.



**Fig. 7** Cell apoptosis induction in MV4-11 cells after treatment with **19**. Treatment with **19** induced apoptosis of MV4-11 cells measured after 48 h.



## Graphical abstract



ACCEPTED

### Highlights

- A class of PRMT5 inhibitors with the IC<sub>50</sub> values ranging from 0.77 to 23 μM were identified.
- The structure-activity relationship (SAR) of this class of structures was discussed.
- The top two active hits (**5** and **19**) showed potent anti-proliferative activity against MV4-11 cells.
- **5** and **19** demonstrated the mechanism of cell killing in cell cycle arrest and apoptotic effect.